3D Deformation of Tensile Cracks in Thin Ductile Sheets: An Optical and Finite Element Investigation

HAREESH V. TIPPUR* and F. P. CHIANG**
*Research Fellow, Graduate Aeronautical Laboratory, California Institute of Technology, Pasadena, CA 91125, USA
**Professor, Laboratory for Experimental Mechanics Research, State University of New York at Stony Brook, Stony Brook, NY 11794, USA

Abstract

3D surface deformations around tensile crack tip in three different types of aluminum sheets is obtained by combined moiré method. Examination of experimental results along with plane stress HRR fields indicate a 3D zone of size varying from 0.75-1.5 sheet thickness around the crack tip. A combined moiré-finite element scheme has been used to calculate deformation fields in the interior of the material. Through-the-thickness variation of strains in the crack tip vicinity support the experimental observations. 3D volume integral J_{local} is calculated through the thickness of the material and its average value is compared with Rice's contour integral J evaluated from the surface deformations.

1 Introduction

It is well known that the crack tip deformation fields are three dimensional in nature although they are often described by two dimensional singular fields due to the lack of 3D closed form solutions. In recent times there has been an increasing interest to establish the zones of 3D deformation and J dominance around tensile crack tip in thin ductile sheets[1-7]. Several experimental and numerical investigations of the deformation fields around the crack tip are reported in the literature. Rosakis and Ravi-Chander[1] have quantified a zone of 3D deformations around an elastically deformed crack tip. Further experimental studies done by Chiang and Hareesh[2] using moiré and laser speckle methods, Zehnder *et.al.*,[3] using caustics have indicated similar 3D zones when the crack tip is surrounded by large plastic zones. Kang *et.al.*,[8] have studied crack blunting and stable crack growth using moiré interferometry. A numerical investigation supplemented with interferometric measurements have indicated 3D deformation fields around ductile crack tip in the works of Narasimhan *et.al.*,[4]. Finite element investigations of Nakamura and Parks[5], Narasimhan *et.al.*,[6] and Hom and McMeeking[7] have also indicated 3D deformation zones in tensile ductile sheets.

In this paper we present complete surface deformation fields around elasto-plastically deformed crack tip using combined moiré method[9] in three different aluminum alloys. 3D deformation zone is experimentally estimated around the crack tip. Experimental results are supplimented with an integrated moiré- finite element investigation[10] of the same specimen geometry.

2 Combined Moiré Method

We have used 'combined moiré method'[9] to obtain simultaneously all the components of surface displacement around a plastically deformed crack tip. The experimental set-up is shown schematically in Fig. 1. The specimen surface is photoprinted with a cross grating of density 40 or 20 lines per mm. This is illuminated by a standing wave created by an optical arrangement whose optical axis makes an angle β with that of the camera axis. The standing wave is created on the surface by a He-Ne laser beam which is first expanded by a microscopic objective and then collimated by a field lens before it impinges upon

a line-grating. The regular and diffracted wavefronts are collected by a second field lens which forms the diffraction spectrum of the grating at its focal plane in the form of a series of equally spaced bright dots called diffraction orders. All the orders are blocked by a mask except the ± 1 orders which are collected by a third field lens to form two nearly collimated beams with an angle 2α between them to impinge upon the specimen. Within the intersecting beams there exists a standing wave of pitch

$$q = \frac{\lambda}{2 \sin \alpha \cos \beta} \tag{1}$$

where λ is the wave length. A typical single exposure recording of all the grating patterns existing on the surface of the specimen is shown in Fig. 2a. The fine dots are the photoprinted gratings which follow the in-plane displacements during deformation process. The low frequency projected gratings (or the standing wave) which modulate the intensity of the photoprinted pattern deforms according to the out-of-plane deformation of the object. Records of the gratings are made before and after subjecting the specimen to mechanical loading. Moiré fringes corresponding to all three displacement components are obtained by superposing the deformed and undeformed gratings. To separate these displacement fields, the matched pair of deformed and undeformed gratings is subjected to optical spatial filtering[11] using a set up shown schematically in Fig. 2b. The diffraction spectrum corresponding the combined grating pattern is shown in Fig 2c. By performing filtering at the diffraction orders corresponding to the frequency of photoprinted grating, in-plane displacement contours (u_1, u_2) can be obtained. If filtering hole is moved to the diffraction order created by the projected gratings out-of-plane displacements contours (u_3) are obtained. The equations govering displacements are

$$u_1 = Np \tag{2}$$

$$u_2 = N'p \tag{3}$$

$$u_3 = N''q/\tan\beta \tag{4}$$

where p is the pitch of the photoprinted grating and N, N', N'' are the corresponding fringe orders.

3 Experiments

Single edge notch (SEN) specimens (Fig. 3a) were made from 3.2mm thick sheets of three aluminum alloys Al 6061-T6, Al 5052-H32 and Al 2024-0. Specimens had a sheet width to thickness ratio of 24 and a crack length of 12.5mm. Both electro-discharge machined notches of width approximately 400μm as well as fatigue cracks have been investigated. Rolling direction of the sheet specimens in all the cases were maintained parallel to the loading axis. By using combined moré method three dimensional surface deformation fields around the crack tip were obtained. In all cases a region of about a square inch around the crack tip was recorded as the specimen underwent monotonically increasing far field tensile load. Typical fringe pattern are shown in Fig. 3b. In these, each of the fringes represent displacement of one pitch in the respective direction [$Al2024-0(\sigma_\infty/\sigma_e = 2.04) : u_1, u_2 = 0.0508$mm/fringe, $u_3 = 0.036$mm/fringe; $Al5052-H32(\sigma_\infty/\sigma_o = 0.88)$ and $Al6061-T6(\sigma_\infty/\sigma_o = 0.67) : u_1, u_2 = 0.0254$mm/fringe, $u_3 = 0.032$mm/fringe]. The non-linear material response of each of these materials was obtained by performing uniaxial tensile tests on specimens made from the same stock of material used for making the SEN specimens. The material response is approximated by the Ramberg-Osgood approximation namely,

$$\frac{\epsilon}{\epsilon_o} = \frac{\sigma}{\sigma_o} + \alpha(\frac{\sigma}{\sigma_o})^n \tag{5}$$

where ϵ_o and σ_o are the reference strain and reference stress and n is the hardening exponent and α is a constant. Material constants for the different alloys used in the study as as follows:

Material	σ_o kg/sq.mm	ϵ_o	α	n
Al 2024-0	5.0	0.00067	1.9	3.05
Al 5052-H32	17.0	0.0023	3.75	7.3
Al 6061-T6	28.0	0.004	1.22	18.0

4 Crack Tip 3D Zone

The experimental measurements have been examined under the presumption that plane stress HRR[12,13]

fields dominate the vicinity of the crack tip. Normalized in-plnae displacements u_2 and out-of-plane displacements u_3 have been compared with the corresponding ones predicted by the HRR equations. Since crack tip damage is characterized by the local parameter namely crack tip opening displacement (CTOD)[14] δ_t, it is used to normalize the displacements. The undeformed sheet thickness h is used as the characteristic length parameter to normalize the radial distance r to bring out the effect of the finite sheet thickness which is responsible for the 3D deformation. The singular field equations used in the process of comparison are:

$$\epsilon_{ij}(r,\theta) = \alpha\epsilon_o[\frac{J}{\alpha\sigma_o\epsilon_o I_n r}]^{\frac{n}{n+1}}\hat{\epsilon}_{ij}(\theta, n) \tag{6}$$

$$u_i(r,\theta) = \alpha\epsilon_o r[\frac{J}{\alpha\sigma_o\epsilon_o I_n r}]^{\frac{n}{n+1}}\hat{u}_i(\theta, n) \tag{7}$$

$$\text{and } \delta_t = (\alpha\epsilon_o)^{\frac{1}{n}} D_n(\frac{J}{\sigma_o}) \tag{8}$$

For plane stress, material incompressibility can be used to approximate

$$\epsilon^p_{33} \approx -\frac{2u_3}{h} = -[\epsilon^p_{rr} + \epsilon^p_{\theta\theta}] \tag{9}$$

Here J is Rice's path independent integral, $\hat{\epsilon}_{ij}$, $\hat{u}_i$ are functions of polar coordinate θ and the hardening exponent of the material while I_n, D_n are dependent on only n. Experimental CTOD was measured by counting the total number of fringes between the lower and the upper lips of the crack up to about 1-2 mm behind the visible crack tip position. It is to be noted that the normalized displacements contain a factor $J^{\frac{1}{n+1}}$. This value of J was estimated using

$$J_{est} = K^2/E \text{ where } K = c\sigma_\infty\sqrt{\pi a'} \tag{10}$$

where a' is Irwin's corrected crack length obtained by taking into account the plastic zone surrounding the crack tip and c is the geometrical factor. This is also estimated by plotting J given by Eqn.(6) for $\epsilon_{22}(\approx$ pitch/fringe spacing) vs r using the opening displacement along $\theta = 0$. The values are then extrapolated to the crack tip from the far field after ignoring the data points in the near vicinity of the crack tip. Figure 4a shows a plot of such a procedure for Al 5052-H32 specimen subjected to a far field stress of $0.88\sigma_o$. Although the above procedures tend to give similar results when the applied load is less than the limit load of the material, the latter is reliable when applied loads are large compared to the limit load. However, it should be pointed out that the errors in estimated J have minimal effect for larger values of n due to the exponentiation. In Fig. 4b plots of normalized displacements vs (r/h) are shown for the same case. It can be observed that the crack tip out-of-plane displacement is finite as against the singular prediction by the HRR model. More interesting is that one can see a general trend in these plots that within a small region near the crack tip displacements predicted by the HRR model deviate substantially from the experimental measurements. This is a result of three dimensional deformation around the crack tip. To estimate the size of this region, we have chosen a criterion that the boundary of 3D effects is at a length r where the difference between the two is greater than or equal to $\pm 0.025\delta_t$. Several experimental measurements for different load levels and different materials were made. A composite of all such measurements is shown in Fig. 5. Within the limits of experimental scatter, these measurements show a regular trend indicating a 3D zone of size $0.75h$ along the crack line and $1.5h$ along approx. 45 degrees. The size of the zone seems to be essentially invariant with respect to the applied load level, material and whether it is a notch or a fatigue crack.

5 Moiré-FE Calculations

Experimental surface measurements have indicated a 3D zone around the crack tip. To confirm this further and investigate the deformation in the interior of the material, we have carried out FE analysis based on deformation theory of plasticity and small strain formulation. Three dimensional FE modelling was done using eight node brick elements with 2 X 2 X 2 gauss integration. The entire thickness of the sheet is cosidered as eight equal thickness layers. Here the FE modelling differs from conventional FE analysis (Fig. 6). Instead of considering a large region R $(=R_1 + R_2)$ so that far field boundary conditions (uniform stress, in this case) is applied, we consider only a small region of interest (R_2) around the crack tip. The boundary nodes of this smaller region are supplied with displacement boundary conditions obtained experimentally from the surface of the sheet using moiré method. Figure 7 shows the fringe

patterns corresponding to the region R_2 around the crack tip. The load level is $0.8\sigma_o$ and material under study is Al 6061-T6. Each of the fringe contours represent a displacement of 25.4μm in the respective direction. The in-plane displacements on the boundary nodes were assumed to be the same for the interior as well as the surface while the thickness change was assumed to have a linear variation with midplane fixed in the x_3 direction. These assumptions are supported from the experimental observations that the deformation fields are generally 2D beyond the 3D zone. This type of FE formulation, 'Hybrid Method', not only reduces the size of the model one has to consider but also provides more reliable deformation fields around the crack tip and cuts down computational effort [10]. The hybrid model we have considered here has 2235 dof and 492 elements. Due to the symmetry of the problem only one quarter of the plate is considered.

Figure 8 shows the contour maps of the dominant strain component ϵ_{22} on the midplane and the surface of the thin sheet (each contour represent a strain of 0.004). Although the distribution near the boundary are same, near the crack tip there are significant differences in the strain values which become apparent from Fig. 9. Figure 9a is the plot of the ratio of midplane ϵ_{22} and surface ϵ_{22} along the crack line $(r, \theta = 0)$. It is to be noted that the values tend to approach unity beyond a distance r=1-1.5 times the thickness of the sheet. Close to the crack tip the ratio is well beyond unity indicating a 3D deformation zone with higher strains on the midplane due to the constraint when compared with the surface. In Fig. 9b through-the-thickness variation of crack tip ϵ_{22} is plotted along the crack front. Strain variation between the interior layers is small with a steep reduction in the surface strain values.

To characterize the amplitude of singularity in non-linear elastic solids J-integral is often used. The local energy release rate J in a 3D solid around a crack front is,

$$J_{\text{local}}(s) = \mu_k(s) \int_\Gamma (W n_k - \sigma_{ij} n_j \frac{\partial u_i}{\partial x_k}) d\Gamma \tag{11}$$

where s denotes the location along the crack front, W is the strain energy density, u_i and σ_{ij} are the cartesian displacement and stress components, n_i are the components of a unit vector normal to Γ and μ_k denotes the local direction of crack advance. The above integral reduces to Rice's J-integral for two dimensional solids. The above formulation is not suitable from the point of view of discrete computations. Alternatively, the numerical formulations of Nakamura *et.al.*, [15] have been used to evaluate J_{local} wherein the above line integral is formulated as a volume integral. Figure 10 shows the calculated values of J_{local} for different layers of the plate considered in this analysis. The value corresponding to the surface was obtained by merely extrapolating the four interior values. The average value of J_{local} is 13.0 kg/mm. Also, Rice's J-integral was calculated from the surface u_2 displacement and ϵ_{22} strain values using the approximate schemes of Kang *et.al*[8]. The J_{local} values on the interior plane are about 1.3 times the ones for first interior layer and 1.5 times the ones for the surface. The average value of J_{local} over the plate thickness seem to be in fairly good agreement with the surface integral value.

6 Conclusions

Experimentally we have been able to map three dimensional surface deformation fields around the crack tip. Experimental measurements have indicated a 3D deformation zone around the crack tip up to about 0.75-1.5 times the undeformed plate thickness. The size of this zone seem to be unaffected by the material hardening exponent, applied load level and undeformed crack tip profile. We have probed the interior of one of the materials, Al 6061-T6, using a combined experimental-finite element scheme. Strain comparison between midplane and surface has again indicated 3D deformations up to about 1.5 times the thickness of the plate beyond which deformation is essentially 2D. Discrete J_{local} have been calculated for different layers of the specimen and its average value is compared with Rice's J-integral calculated using only the surface data. Good agreement between the two is obtained.

Acknowledgements

Research was performed at the Laboratory of Experimental Mechanics Research, S.U.N.Y at Stony Brook when Hareesh V. Tippur was a Graduate Student. Work supported by ONR Mechanics Division (Dr. Y. Rajapakse, Scientific Officer) Contract No. N0001482K05066 and NSF Solid and Geo-Mechanics Program (Dr. K. Thirumalai, Program Director), Grant No. MEA4803912. Dr. T. Nakamura's help in the computational aspects of the work is appreciated.

References

1. Rosakis, A.J. and Ravi-Chandar, K., 'On the Crack Tip Stress State: An Experimental Evaluation of Three Dimensional Effects', International Journal of Solids and Structures, Vol.22, 1986, pp 121-134.

2. Chiang, F.P. and Hareesh, T.V., 'Three Dimensional Crack Tip Deformation: An Experimental Study and Comparison to HRR Field', Intl. J. of Fracture, Vol. 36, pp 243-257, 1988.

3. Zehnder, A.T., Rosakis, A.J. and Narasimhan, R., 'Measurement of the J-integral with Caustics: An Experimental and Numerical Investigation', GALCIT Report 86-8, California Institute of Technology, 1986.

4. Narasimhan, R., Rosakis, A.J. and Zehnder A.T., '3D Fields for a Through Crack in an Elastic-Plastic Solid: Numerical Analaysis and Comparison with Interferometric Measurements', Proc. of the Symposium on Analytical, Numerical and Experimental Aspects of 3D Fracture Processes, Joint ASME/SEM Conference, Berkeley, CA, 1988.

5. Nakamura, T. and Parks, D.M., 'Three-Dimensional Stress Field Near the Crack Front of a Thin Elastic Plate', M.I.T. Report, 1987.

6. Narasimhan, R. and Rosakis, A.J., 'A Finite Element Analysis of Small Scale Yielding Near a Stationary Crack under Plane Stress', Journal of the Mechanics and Physics of Solids, 1988.

7. Hom, C.L. and and McMeeking, R.M., 'Large Crack Tip Opening in Thin Elasto-Plastic Sheets', Technical Report, Univ. of California, Santa Barbara, 1987.

8. Kang, B.S.-J., Kobayashi, A.S. and Post, D., 'Stable Crack Growth in Aluminum Specimens', Vol. 27, No. 3, Experimental Mechanics, pp 234-245, 1987.

9. Tippur, V. Hareesh 'Mapping Elasto-Plastic Deformations Using Optical and Numercal Methods', Ph.D. Thesis, Dept. of Mechanical Engineering, S.U.N.Y. at Stony Brook, 1988.

10. Hareesh, T.V. and Chiang, F.P., 'Integrated Optical-Finite Element Approach for Studying Elasto-Plastic Crack Tip Fields', S.U.N.Y. at Stony Brook Technical Report No. 483, (to appear in the J. of Engineering Fracture Mechanics, 1988), 1987.

11. Chiang, F.P., 'Multi-purpose Optical Moiré Processor', Optical Engineering, Vol. 18, No. 5, pp 456-460, 1979.

12. Hutchinson, J.W., 'Singular Behavior at the End of a Tensile Crack in a Hardening Material', J. of the Mechanics and Physics of Solids, Vol. 16, pp 64-75, 1968.

13. Rice, J.R., and Rosengren, G.F., 'Plane Strain Deformation Near a Crack Tip in a Power-law Hardeing Material', J. of the Mechanics and Physics of Solids, Vol. 12, pp 353-364, 1968.

14. Shih, C.F., 'Relationship Between the J-integral and the Crack Opening Displacement for Stationary and Extending Cracks', J. of the Mechanics and Physics of Solids, Vol. 29, No. 4, pp 305-326, 1981.

15. Nakamura, T., Shih, C.F. and Freund, L.B., 'Three Dimensional Transient Analysis of a Dynamically Loaded Three-Point-Bend Ductile Fracture Specimen', Brown Univ. Report ONR0365/3, 1986.

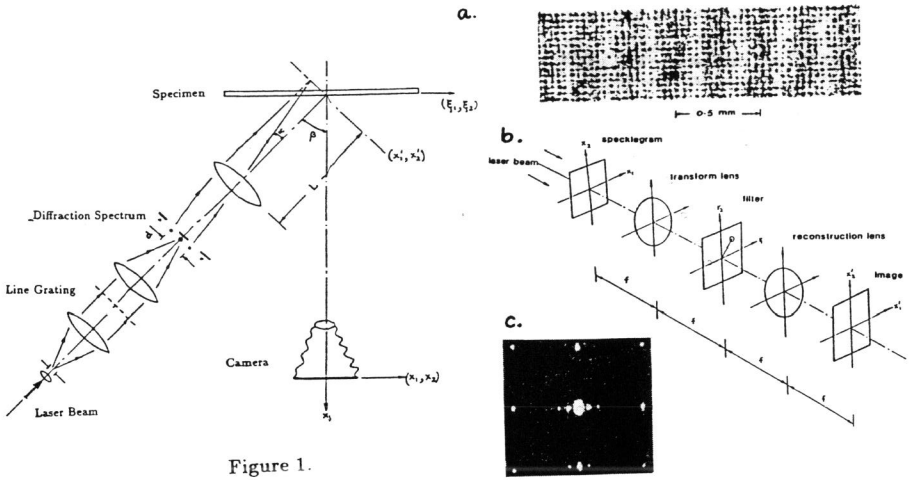

Figure 1.

Figure 2.

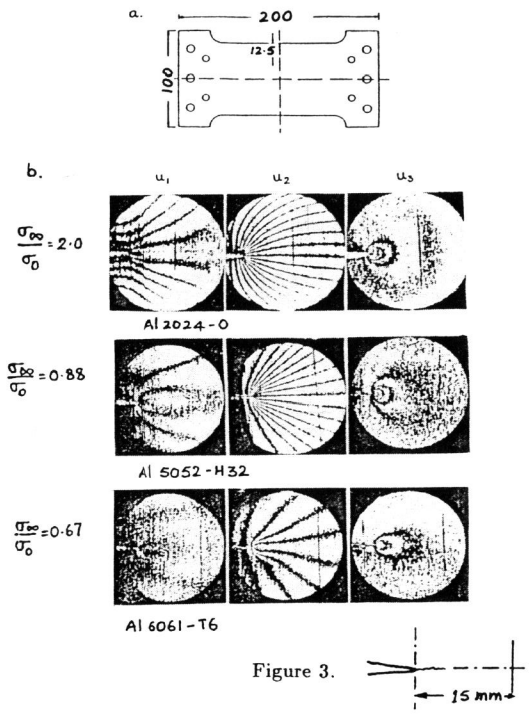

Figure 3.

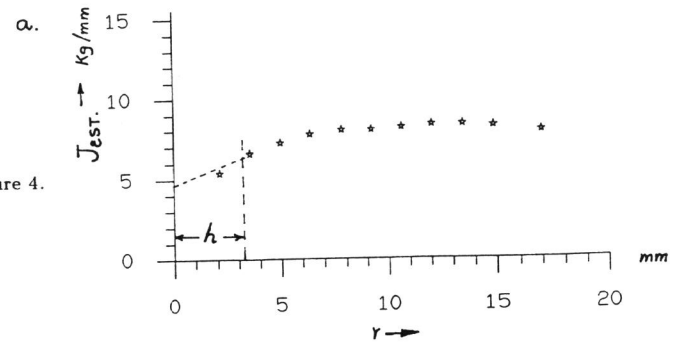

Figure 4.

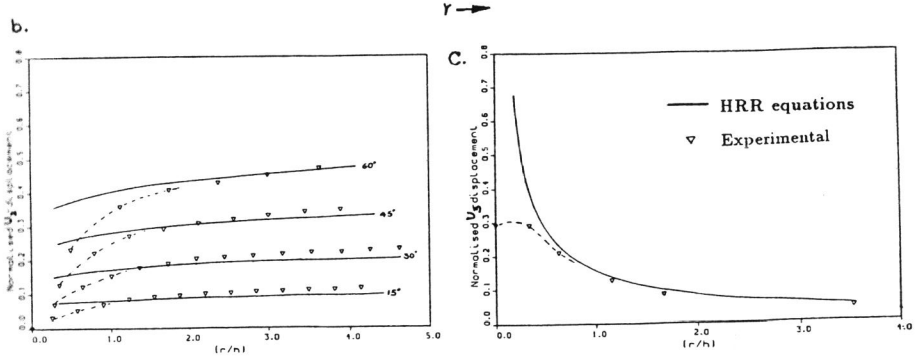

Figure 5.

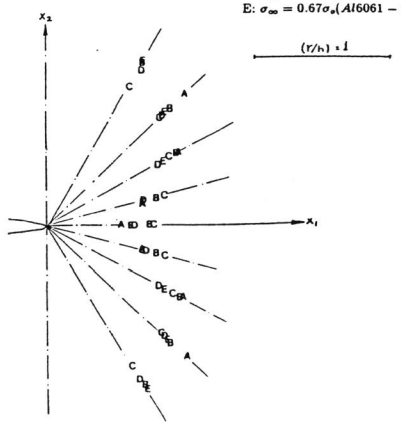

Figure 6.

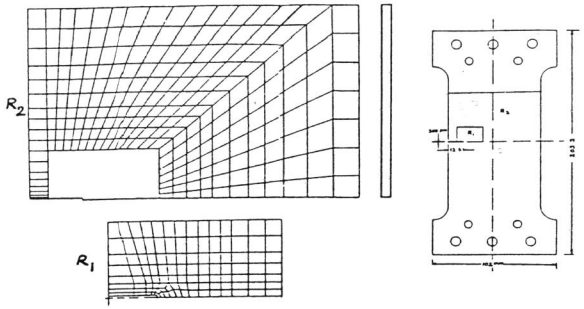

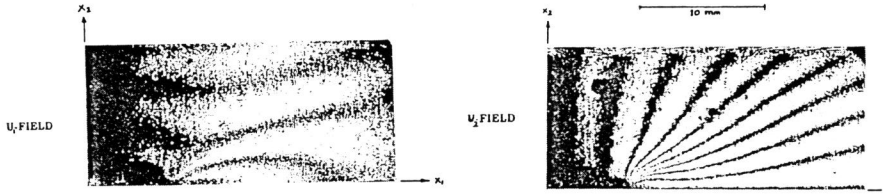

Figure 7.

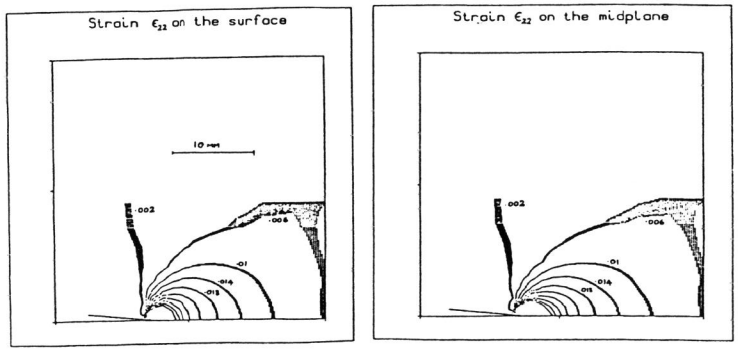

Figure 8.

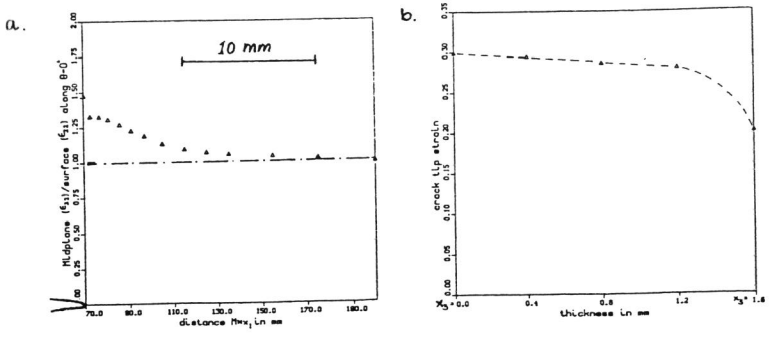

Figure 9.

Figure 10.

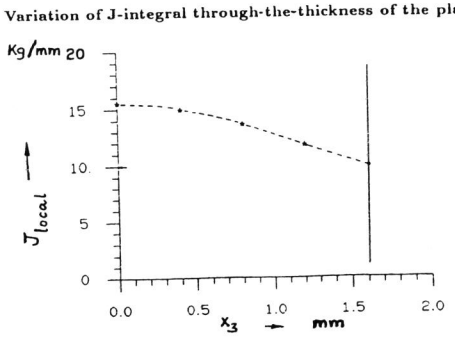

Average J_{local}[ref.15]=13.0 kg/mm
Rice's J (experimental)[ref.8]=11.24 kg/mm
Rice's J (hybrid method)[ref.8]=11.0 kg/mm